Article:
Raines, Daniel J., Clarke, Justin E., Blagova, Elena V. et al. (2018) Redox-switchable siderophore anchor enables reversible artificial metalloenzyme assembly. Nature Catalysis. pp. 680-688. ISSN: 2520-1158

https://doi.org/10.1038/s41929-018-0124-3

Redox-switchable Siderophore Anchor Enables Reversible Artificial Metalloenzyme Assembly

Daniel J. Raines,[1] Justin E. Clarke,[1,2] Elena V. Blagova,[2] Eleanor J. Dodson,[2] Keith S. Wilson[2]* and Anne-K. Duhme-Klair[1]*

[1]Department of Chemistry, University of York, Heslington, York, YO10 5DD, United Kingdom

[2]Structural Biology Laboratory, Department of Chemistry, University of York, Heslington, York, YO10 5DD, United Kingdom

*e-mail: keith.wilson@york.ac.uk, anne.duhme-klair@york.ac.uk

---

ABSTRACT:

Artificial metalloenzymes that contain protein-anchored synthetic catalysts are attracting increasing interest. An exciting, but still unrealised advantage of non-covalent anchoring is its potential for reversibility and thus component recycling. Here we present a siderophore-protein combination that enables strong but redox-reversible catalyst anchoring, as exemplified by an artificial transfer hydrogenase (ATHase). By linking the iron(III)-binding siderophore azotochelin to an iridium-containing imine-reduction catalyst that produces racemic product in the absence of the protein CeuE, but a reproducible enantiomeric excess if protein bound, the assembly and reductively-triggered disassembly of the ATHase was achieved. The crystal structure of the ATHase identified the residues involved in high-affinity binding and enantioselectivity. Whilst in the presence of iron(III) the azotochelin-based anchor binds CeuE with high affinity, the reduction of the coordinated iron(III) to iron(II) triggers its dissociation from the protein. Thus, the assembly of the artificial enzyme can be controlled *via* the iron oxidation state.

The development of artificial metalloenzymes is a rapidly expanding field, with design strategies ranging from the modification of natural metalloenzymes through to complete *de novo* design (Fig. 1a).[1-7] Of these, the anchoring strategy, in which a synthetic catalyst is attached to a protein scaffold, has drawn much attention since it allows the reactivity of organometallic catalysts to be harnessed in a biocompatible and (stereo)selective protein environment.[8-10] In contrast to covalent anchoring, non-covalent anchoring does not rely on reactive functional groups for bond formation, and hence it allows the individual components, in particular the catalytic site and the protein scaffold to be optimised independently, before the artificial enzyme is assembled and further optimised as a whole.[8, 11, 12] This advantage of non-covalent anchoring has been exploited extensively, mainly by utilising the streptavidin-biotin affinity pair,[8, 13-16] while enzyme-inhibitor and myoglobin-heme combinations[17-19] have also been explored.

Whilst these affinity pairs benefit from the enormous binding strength that cooperative non-covalent interactions can confer, their potential for controlled reversibility has not yet been accomplished. Yet, anchoring should be a reversible process that allows the anchor to be detached when required. Hence, for modularly-designed artificial enzymes to reach their full potential, a strong but reversible anchoring process is required, which enables both the controlled assembly and disassembly of the components. Controlled reversibility would allow the recycling of both protein scaffold and artificial metal cofactor. The controlled release and replacement of a catalyst should enable exciting new applications in biosensing and (micro)fluidic devices, especially when the protein scaffold is immobilised. Hence, much effort has been devoted to achieving reversibility with biotin derivatives[20] and alternatives[21] or (strept)avidin mutants,[22] but the necessary fine tuning of the hydrogen bonding network is challenging.

Siderophores and their cognate periplasmic binding proteins (PBPs)[23] on the other hand, have properties that are well suited to the development of redox-reversible anchoring systems. Siderophores are produced by microorganisms for the uptake of essential iron(III) and the iron complexes of siderophores are bound strongly, but reversibly, by their cognate PBPs.[24-27] Inside the cell, the prominent mechanism for the release of iron from siderophores is reduction of the coordinated iron(III) to iron(II). Iron release from the siderophore is facilitated asthe resulting iron(II)-siderophore complexes have a lower thermodynamic stability and are kinetically more labile than their Fe(III) counterparts.[25, 26, 28] We previously reported that CeuE, an iron-siderophore PBP of *Campylobacter jejuni*, has high affinity for the iron(III) complex of the tetradentate siderophore bis(2, 3-dihydroxy-benzoyl-L-Ser) (H_5-bisDHBS, **1**, Fig. 1b), based on the direct metal coordination by two amino acids, His227 and Tyr288.[29, 30]

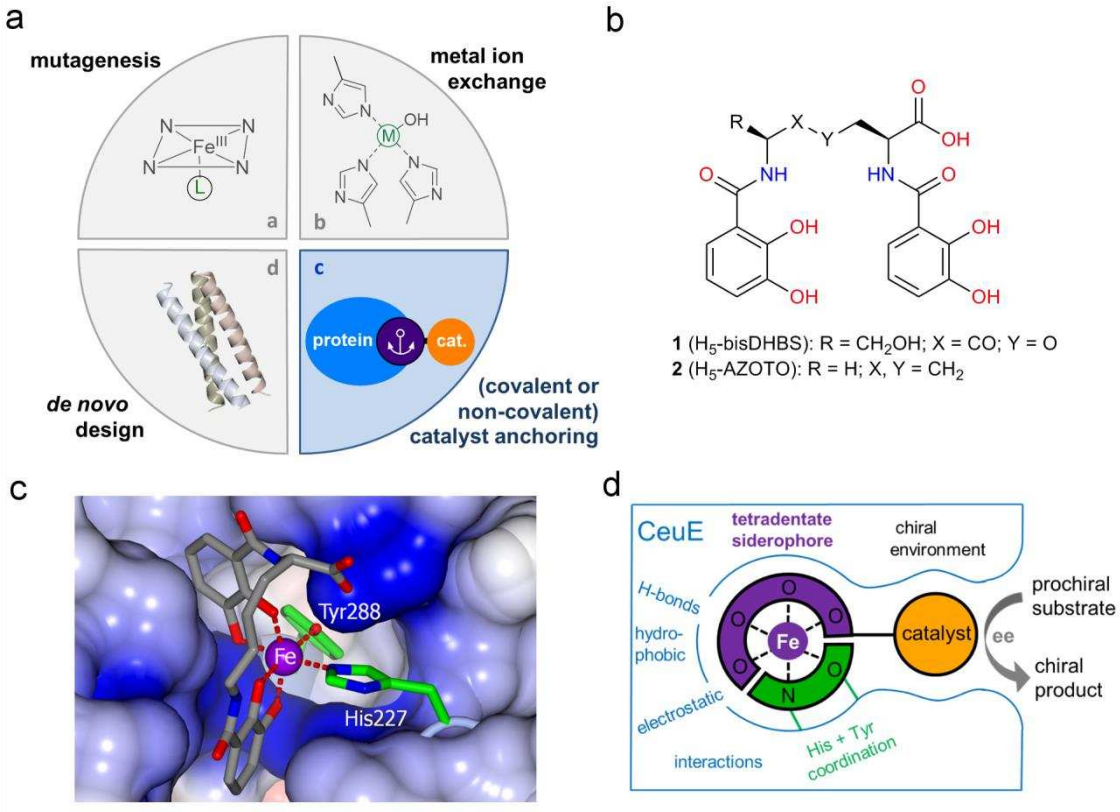

Figure 1. Design considerations. a, Strategies for the development of artificial metalloenzymes. **b**, Structures of bis(2, 3-dihydroxy-benzoyl-L-Ser) (H_5-bisDHBS) **1**, and azotochelin (H_5-AZOTO) **2**. **c**, Detail of the crystal structure of $[Fe^{III}(AZOTO)]^{2-}$⊂CeuE (PDB 5OAH) illustrating tetradentate siderophore binding. Two protein side chains, Tyr288 and His227, complete the coordination sphere of the iron (CeuE: electrostatic surface representation; Fe purple; C green (His227, Tyr288) or grey (azotochelin); remaining atoms of siderophore and Fe-coordinating residues coloured by atom type). **d**, Siderophore-anchored metalloenzyme design: CeuE (blue and green), iron(III) complex of a tetradentate siderophore (purple) and attached transfer hydrogenation catalyst (orange).

Here we show how this binding mode can be exploited in the development of a redox-switchable iron-siderophore anchor that allows the reversible attachment of synthetic catalysts to CeuE. To monitor whether the synthetic catalyst is turning over in its protein-bound form or, after release, in its unbound state, we chose the transfer hydrogenation of a pro-chiral imine as indicator reaction and a racemate-producing organometallic complex as the initial model catalyst. In this system, the interactions of the catalyst with the chiral protein scaffold are reflected in the level of enantioselectivity observed. The choice of catalyst was based on the suitability of similar catalysts in the development of previously reported enantioselective artificial transfer hydrogenases.[31-33]

RESULTS

Anchor Design.

Since the tetradentate siderophore **1** that we studied initially is challenging to synthesise and hydrolytically unstable, azotochelin, **2** (Fig. 1b), the siderophore of *Azotobacter vinelandii* was

selected instead. Azotochelin was synthesised as previously described[34] and the affinity of its Fe(III) complex for CeuE was determined *via* intrinsic fluorescence quenching (see Supplementary Methods). With 4.9 ± 0.4 nM, its dissociation constant compares favourably with those reported for artificial enzymes that rely on biotin as anchoring unit (e.g. biotinylated Hoveyda-Grubbs catalyst⊂avidin: K_d = 6.3 nM)[35] or enzyme inhibitors (e.g. sulfonamide-bearing transfer hydrogenation catalyst⊂hCA II: K_d = 15 nM).[17] In contrast, the affinities of apo-azotochelin and Fe(II)-azotochelin for CeuE were too low to be determined in this concentration range (K_d = >1 μM, Supplementary Fig 1).

To reveal the interactions between $[Fe^{III}(AZOTO)]^{2-}$ and CeuE, $[Fe^{III}(AZOTO)]^{2-}$ was soaked into crystals of apo-CeuE (PDB code 3ZKW) and the structure of the resulting complex, $[Fe^{III}(AZOTO)]^{2-}$⊂CeuE, was determined. The structure (PDB code 5OAH, Supplementary Methods and Supplementary Fig. 2) showed that the four catecholate oxygen donors of azotochelin coordinate to the Fe(III) centre with the remaining coordination sites being occupied by the donors of His227 and Tyr288 (Fig. 1c). The carboxylate group in the backbone of the siderophore was deemed appropriate as a conjugation site for the attachment of a catalyst since it remains uncoordinated and points away from the binding site.

The reductively-triggered dissociation of the iron(III) complex of azotochelin was then investigated (Fig. 2). First, the iron(III) centre of $[Fe^{III}(AZOTO)]^{2-}$⊂CeuE was reduced to iron(II) by addition of sodium dithionite, as evidenced by the bleaching of the broad catecholate-to-iron(III) charge transfer band in the electronic absorption spectrum of the complex (λ_{max} 547 nm, Fig. 2a). The subsequent addition of an aliquot of the reduced sample (Fig. 2b) to ferrozine,[28, 36] an iron(II) indicator, led to the formation of the intensely-coloured magenta iron(II)-ferrozine complex (Fig. 2c, d), confirming that the reduction to iron(II) is followed by its dissociation from both the siderophore anchor and CeuE. The re-oxidation of iron(II) to iron(III) was achieved by exposure to air and the reassembly of the azotochelin complex was confirmed by

the reappearance of its characteristic absorption band. The absorption maximum at 543 nm resembles that of $[Fe(AZOTO)]^{2-}\subset$CeuE (λ_{max} 547 nm) rather than that of free $[Fe(AZOTO)]^{2-}$ (λ_{max} 572 nm). Addition of ferrozine to the re-oxidised solution confirmed the absence of residual iron(II) (Fig. 2e).

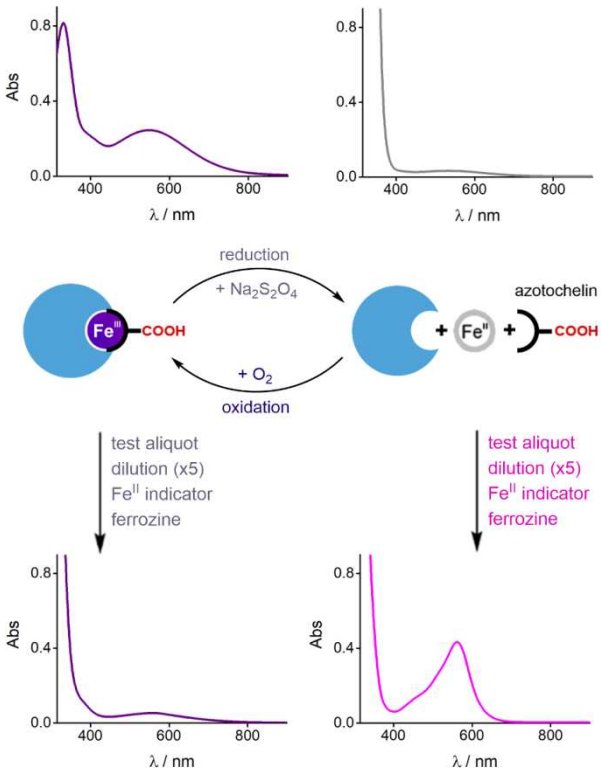

Figure 2. Redox-switchable siderophore anchoring. a-e. Reductively-triggered dissociation of $[Fe^{III}(AZOTO)]^{2-}\subset$CeuE and its oxidatively-triggered reassembly, 0.1 M MES, 0.5 M NaCl, pH 6.0: CeuE (blue), iron(III) (purple), azotochelin (black + red), iron(II) (white/grey), as monitored by visible absorption spectroscopy ($[Fe^{III}(AZOTO)]^{2-}\subset$CeuE: λ_{max} = 547 nm, Fe(II)-ferrozine: λ_{max} 563 nm). Due to the intense magenta colour of the iron(II)-ferrozine indicator complex, the samples containing ferrozine were diluted (5x) to allow for absorption-spectroscopic analysis.

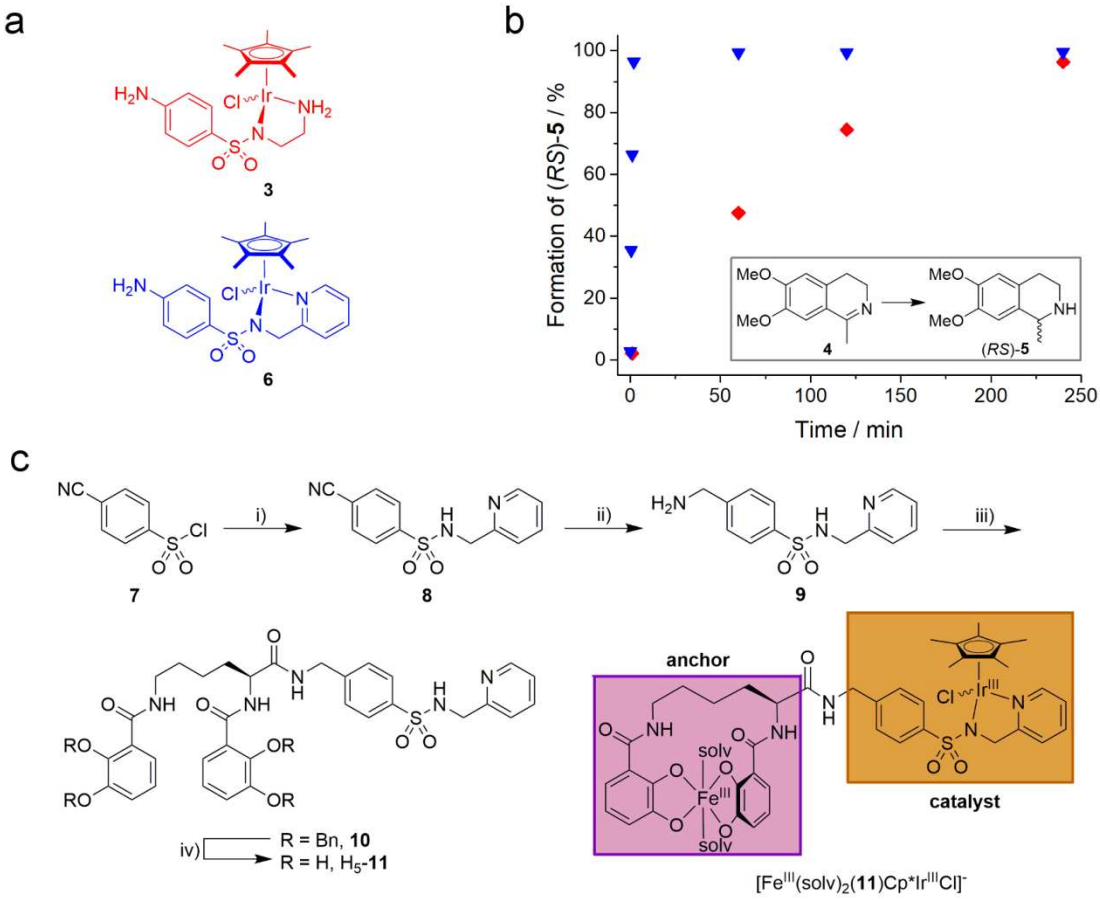

Figure 3. Catalyst development and conjugate synthesis. a, Structures of transfer hydrogenation catalysts **3** and **6**. **b**, Kinetic profiles for the reduction of **4** (50 mM) to (*RS*)-**5** for catalysts **3** (red diamonds) and **6** (blue triangles), both at 0.5 mM in 0.6 M MES, pH 6.5, 3 M sodium formate, 40 °C. **c**, Synthesis of conjugate H_5-**11** and $[Fe^{III}(solv)_2(\mathbf{11})Cp^*Ir^{III}Cl]^-$, with solv = solvent molecule. Conditions: i) 2-(aminomethyl)pyridine, NEt_3, CH_2Cl_2, 78%; ii) $LiBH_4$, MeOH, THF, 68%; iii) Bn_4-AZOTO, EDC, HOBt, NEt_3, DMF, 47%; iv) H_2, Pd-$(OH)_2$/C 20%, EtOH, 95%.

Design, Synthesis and Characterisation of the Artificial Transfer Hydrogenase. Inspired by previous work on ATHases by Ward *et al.,*[8] we initially prepared the Noyori-Ikariya-type catalyst **3**, which was able to catalyse the reduction of **4** to (*RS*)-salsolidine (**5**), but the slow reaction rate was impractical (Fig. 3b). In search of a more active catalyst, we considered

[Cp*Ir(pyridinesulfonamide)Cl] complexes, which have shown promise in the transfer hydrogenation of ketones and aldehydes with 2-propanol.[37, 38] Encouraged by studies reported by Sadler *et al.*[39] and Wills *et al.*,[40] we reasoned that for the reduction of **4** at pH 6.5, an iridium-coordinated amine group would not be required as proton donor. Under these conditions, **4** is protonated and could either react directly with a metal-coordinated hydride[39] or hydrogen bond with the sulfonyl group of the ligand.[41] Hence we replaced the amine group in **3** with a pyridyl group **6** (Fig. 3a). In comparison with **3**, **6** shows a significantly enhanced reaction rate for the reduction of **4** to (*RS*)-**5** (Fig. 3b).

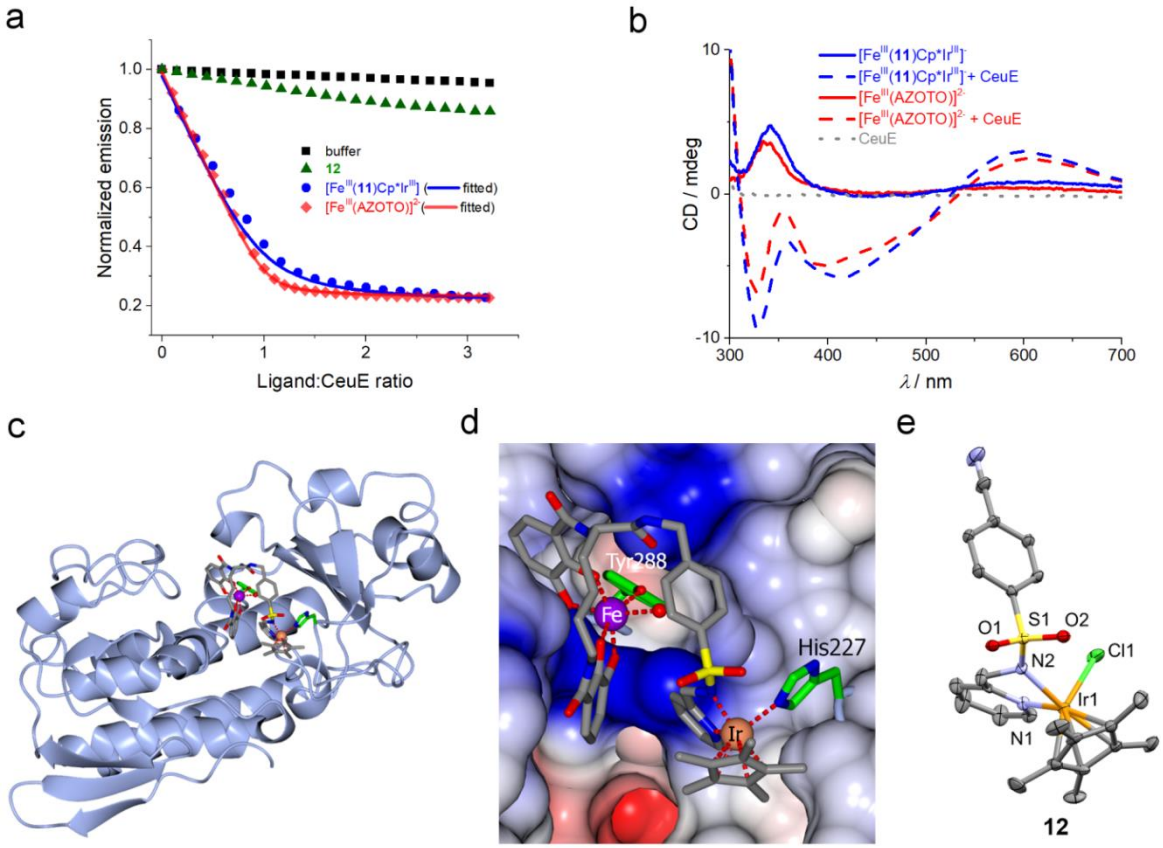

Figure 4. Characterisation of [Fe^{III}(AZOTO)]$^{2-}$⊂CeuE and [Fe^{III}(11)Cp*Ir^{III}]⊂CeuE. a, Fluorescent quenching observed upon addition of [Fe^{III}(AZOTO)]$^{2-}$, [Fe^{III}(**11**)Cp*Ir^{III}] or **12** to CeuE (40 mM Tris-Cl pH 7.5, 150 mM NaCl). **b**, CD spectra of [Fe^{III}(AZOTO)]$^{2-}$ and [Fe^{III}(**11**)Cp*Ir^{III}] in the presence or absence of CeuE, with a control spectrum for CeuE alone. **c**, Crystal struc-

ture of [Fe^{III}(**11**)Cp*Ir^{III}]⊂CeuE (PDB code 5OD5; CeuE ribbon representation; Fe purple; Ir coral; C green (His227, Tyr288) or grey (**11**, Cp*) remaining atoms coloured by type). **d**, Detail of the crystal structure of [Fe^{III}(**11**)Cp*Ir^{III}]⊂CeuE (CeuE: electrostatic surface representation). **e**, ORTEP plot of (*R*)-[Cp*Ir^{III}(**8**)Cl], **12** (50% probability ellipsoids, H atoms omitted for clarity, CCDC 1551724).

To improve the nucleophilicity of the nitrogen atom in **6**, a methylene group was inserted to give **9,** with which the amide bond formation to produce **10** proceeded in good yields (Fig. 3c). [Fe^{III}(solv)$_2$(**11**)Cp*Ir^{III}Cl]$^-$ was obtained by reacting the deprotected conjugate H_5-**11** with iron(III), followed by iridium(III).

Finally, CeuE was added to prepare the ATHase, which was characterised by electrospray ionisation mass spectrometry (ESI-MS; Supplementary Methods, Supplementary Fig. 3). Signals at 32024.4 and 33078.4 Da are consistent with CeuE and [Fe^{III}(**11**)Cp*Ir^{III}]⊂CeuE (theoretical average molecular masses of 32024.0 and 33079.0 Da, respectively). Interestingly, the mass spectra suggest loss of the iridium-coordinated chloride ligand upon protein binding. The dissociation constant of [Fe^{III}(**11**)Cp*Ir^{III}]⊂CeuE confirmed that the iron-siderophore anchor of the conjugate still binds CeuE with suitably high affinity (K_d = 18.3 ± 4.9 nM, Fig. 4a).

In view of the envisaged application of the artificial enzyme in asymmetric catalysis, it was of interest to investigate the stereochemistry of the conjugate. In [Fe^{III}(**11**)Cp*Ir^{III}]⊂CeuE the iron and iridium centres can adopt Λ/Δ- or R/S-configurations, respectively, with the diastereomeric ratio affected by both intramolecular asymmetric induction by the L-lysine backbone and the interactions with the chiral protein binding pocket. It was previously observed that CeuE drives the diastereomeric equilibration of [Fe(bisDHBS)]$^{2-}$ by selecting for Λ-configured iron(III) catecholates.[29, 30, 42, 43] Therefore, we probed the stereochemistry of the metal centres in [Fe^{III}(AZOTO)]$^{2-}$ and [Fe^{III}(solv)$_2$(**11**)Cp*Ir^{III}Cl]$^-$ by recording circular dichroism (CD) spectra,

both in the absence and presence of CeuE. In the absence of CeuE, the CD spectra of both complexes display a positive band between 330 nm and 335 nm and a very weak positive band at around 600 nm (Fig. 4b), which can be assigned to ligand-based transitions and ligand-to-metal charge-transfer (LMCT) transitions, respectively.[44] Since the latter reflect the chirality at the iron(III) centre, the low intensity of the LMCT band is indicative of a weak asymmetric induction effect exerted by the L-lysine backbone in $[Fe^{III}(AZOTO)]^{2-}$ and $[Fe^{III}(solv)_2(\mathbf{11})Cp^*Ir^{III}Cl]^-$.

In contrast, in the presence of CeuE, the CD spectra of $[Fe^{III}(AZOTO)]^{2-}\subset$CeuE and $[Fe^{III}(\mathbf{11})Cp^*Ir^{III}]\subset$CeuE show features consistent with the majority of the iron(III) centres adopting Λ-configuration[44] and confirm that the diastereomers in solution equilibrate quickly. Unfortunately, assignment of configuration to the iridium centre in $[Fe^{III}(\mathbf{11})Cp^*Ir^{III}]\subset$CeuE was prevented by the dominant iron-azotochelin chromophore.

Crystal Structure of $[Fe^{III}(\mathbf{11})Cp^*Ir^{III}]\subset$CeuE. $[Fe^{III}(solv)_2(\mathbf{11})Cp^*Ir^{III}Cl]^-$ was soaked into a crystal of apo-CeuE (PDB code 3ZKW) and the structure was determined by X-ray crystallography. Experimental details are provided in the Supplementary Methods. The crystal is in space group P1 with three independent protein chains (A, B and C) in the asymmetric unit. The following description focuses on chain C, which shows the clearest additional electron density in the binding pocket (Fig. 4c, d).

As seen previously, the azotochelin moiety chelates a Λ-configured iron centre.[29, 30] However, the flexible loop containing His227, which coordinates to the iron in $[Fe^{III}(AZOTO)]^{2-}\subset$CeuE, is displaced by the catalyst and the sixth coordination site is occupied by an aqua/hydroxo ligand.

While the azotochelin moiety is well-ordered and modelled with full occupancy, the catalyst moiety of $[Fe^{III}(\mathbf{11})Cp^*Ir^{III}]$ adopts more than one conformation, evidenced by the anomalous

difference map (Supplementary Fig 4). The major conformation of the catalyst moiety was modelled with an occupancy of 0.6.

The crystal structure of a related iridium catalyst was independently determined (**12**, Fig. 4e, CCDC 1551724) in a centric space group which thus contained both enantiomers. The geometric parameters from this structure were used as restraints in the building and refinement of the conjugate complex model. During the modelling of the major conformation, we were encouraged to find that only one enantiomer gave a satisfactory fit to the density. This provides a potential explanation for the observed enantioselectivity of the protein-bound catalyst (*vide infra*), the protein imposing a preference for one of the two chiral forms. While the electron density is low for the Cp* ring and parts of the catalyst, difference maps confirmed their approximate location (Supplementary Fig. 5). Similar partial occupancies have previously been observed in crystal structures of ATHases with anchored iridium-based catalysts.[17, 32]

In [Fe^{III}(**11**)Cp*Ir^{III}]⊂CeuE, His227 cannot coordinate to the iron since its access is blocked by the catalyst, and instead appears to lie close to the iridium centre and may well be coordinated to it (Supplementary Fig. 6). If it is coordinated, one of the ligands, most likely His227, is required to dissociate to enable hydride coordination during catalysis, and the flexibility of the loop on which His227 is located may make such a movement possible. There is no indication in the structure of an iridium-bound chloride ion, consistent with the mass spectrometry results. Interestingly, dual anchoring *via* coordination of a suitably-positioned histidine residue to the catalyst was previously reported to enhance the enantioselectivity of a biotin-anchored ATHase.[31] In that study, the catalyst was linked to the biotin anchor through the Cp* ligand and the histidine remains coordinated during the catalytic cycle, with the incoming hydride replacing an iridium-bound chloride ligand instead.

Transfer Hydrogenation Catalysis. Catalytic activity tests confirmed that [Fe^{III}(**11**)Cp*Ir^{III}]⊂CeuE is able to catalyse the reduction of **4** to **5**, with the reaction reaching completion within 24 hours (Table 1). The turnover frequency (TOF) is around 20-fold lower than the TOF achieved with [$Fe^{III}(solv)_2$(**11**)Cp*$Ir^{III}Cl]^-$ in the absence of CeuE, consistent with His227 either competing with the hydride for iridium binding and/or sterically restricting the access of the substrate. However, some of the activity decrease is due to the conjugation of the catalyst to the anchor, as reflected by the lower activity of [$Fe^{III}(solv)_2$(**11**)Cp*$Ir^{III}Cl]^-$ compared with **6**. In addition, the presence of the protein causes a reduction in activity for both **6** and [$Fe^{III}(solv)_2$(**11**)Cp*$Ir^{III}Cl]^-$.

Table 1. Catalytic activity towards reduction of 4 to 5.

Catalyst	TOF/min^{-1}	t[a]/h	*ee*[b]/%
6	25.1 ± 0.3 (5 min)	1	< 3
6 + CeuE	5.9 ± 0.1 (15 min)	4	< 3
[$Fe(solv)_2$(**11**)Cp*IrCl]$^-$	6.0 ± 0.3 (15 min)	4	< 3
[Fe(**11**)Cp*Ir]⊂CeuE	0.30 ± 0.01 (8 h)	24	35.4 ± 0.1 (*R*)
[Fe(**11**)Cp*Ir]⊂H227A	2.0 ± 0.2 (2 h)	8	3.3 ± 0.5 (*R*)

0.6 M MES buffer, pH 6, 3 M HCOONa, 40 °C, 50 mM substrate, 0.125 mM catalyst, measurements were carried out as independent triplicates, the uncertainty in the average is indicated as (range/2)/(SQRT(3)), TON at completion: 400. [a]Time to completion. [b]Enantiomeric excess (*ee*) assigned by comparison with an enantiomerically-pure standard.

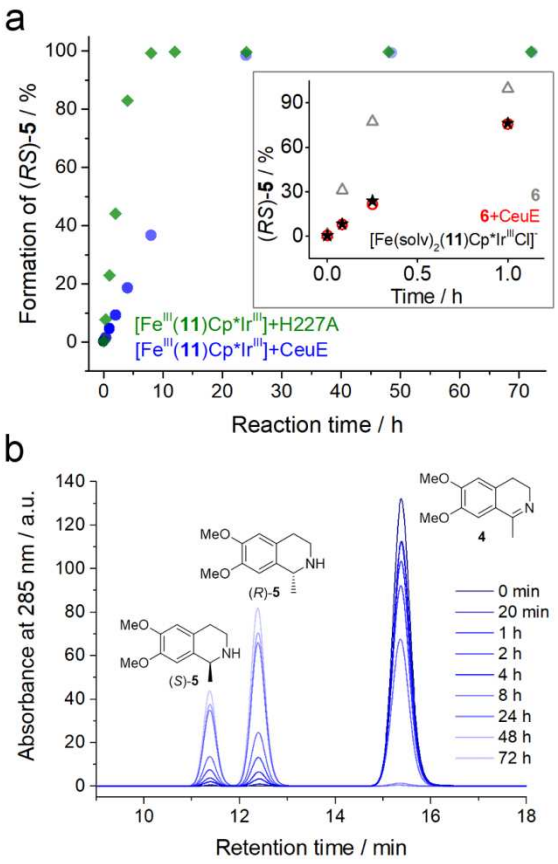

Figure 5. Catalytic activity of [Fe^{III}(11)Cp*Ir^{III}]⊂CeuE and control compounds. a, Kinetic profile for the formation of (*RS*)-**5** catalysed by [Fe^{III}(**11**)Cp*Ir^{III}]⊂CeuE (blue circles) and [Fe^{III}(**11**)Cp*Ir^{III}]⊂H227A (green diamonds). Kinetic profiles of control reactions with **6** (grey hollow triangles), **6** + CeuE (red hollow circles) and [Fe^{III}(solv)$_2$(**11**)Cp*Ir^{III}Cl]$^-$ (black stars) over a shorter time scale are shown in the inset. **b**, Chiral HPLC traces obtained during the reduction of **4** (50 mM) to (*R*)- and (*S*)-**5** catalysed by [Fe^{III}(**11**)Cp*Ir^{III}]⊂CeuE, 0.125 mM (0.25 mol%) in 0.6 M MES pH 6, 3 M HCOONa, 40 °C.

Nevertheless it is encouraging that [Fe^{III}(**11**)Cp*Ir^{III}]⊂CeuE shows significant and reproducible enantioselectivity in favour of the (*R*) enantiomer of **5**. The enantiomeric excess obtained (*ee* 35%) lies within the range reported for other ATHases prior to genetic optimisation.[17, 32, 45] If **6** is used in the presence of CeuE, (*R*)-**5** and (*S*)-**5** are produced unselectively (Table 1). A similar lack of enantioselectivity is seen when [Fe^{III}(solv)$_2$(**11**)Cp*Ir^{III}Cl]$^-$ is used in the absence of

CeuE. Hence, chiral induction by the L-lysine backbone of azotochelin is insignificant. These observations confirm that the siderophore-mediated anchoring to CeuE is required to achieve enantioselectivity, since it positions the catalyst within the chiral environment provided by the protein. To gauge the contribution of the His227 to the enantioselectivity, it was replaced with a non-coordinating residue, as previously described.[43] The mutation of His227 to alanine (H227A) resulted in a clear drop in the *ee* to approximately 3%, whilst the catalytic rate increased to around a third of the free conjugate. This suggests that whilst His227 impedes the catalysis to a significant extent, potentially by coordinating to the iridium centre, it is responsible for a large portion of the enantioselectivity.

Release of the Siderophore-anchored Catalyst and ATHase Re-assembly . Sodium dithionite was added to [Fe^{III}(**11**)Cp*Ir^{III}]⊂CeuE until the bleaching of the catecholate-to-iron(III) charge-transfer band confirmed that the reduction had gone to completion (λ_{max} 547 nm, Fig. 6a-c and Supplementary Fig. 7). The separation of the reductively released iron(II) and the azotochelin-catalyst conjugate from CeuE was achieved by centrifugal microfiltration (details in the Supplementary Methods). Once SDS-PAGE (Supplementary Fig. 8a), CD (Supplementary Fig. 8b) and UV/vis spectroscopy confirmed that the recovered CeuE was intact, correctly folded and free of residual azotochelin-catalyst conjugate, [Fe^{III}(**11**)Cp*Ir^{III}]⊂CeuE was reassembled by addition of a fresh aliquot of [Fe^{III}(solv)$_2$(**11**)Cp*Ir^{III}Cl]$^-$. The activity of the reassembled ATHase was confirmed in subsequent catalytic runs. Whilst the %conversion obtained with the recycled protein was slightly lower than that seen pre-recycling, the stereo-directing effect of the protein was fully restored (*ee* 32%, Fig. 6d).

The recovery of the azotochelin-catalyst conjugate from the spin filtrate proved challenging due to adsorption by the semipermeable membrane of the cut-off filter. If required, it is possible to partially recover functional catalyst conjugate by extraction of the reduced artificial en-

zyme solution with ethyl acetate, followed by HPLC (Recovery yields: iridium-bound azotochelin-catalyst conjugate 11%, H_5-**11** 15%; Supplementary Methods, Supplementary Fig. 9). However, the extraction with ethyl acetate leads to the precipitation of CeuE and the recovery yield is low. Consequently, the current system allows the recycling of either the protein or a fraction of the conjugate, but not both at the same time.

Further recycling studies are underway and are directed towards siderophore-catalyst conjugates, in which the catalyst is linked to the siderophore through the Cp ligand. The aim is to not only improve the solubility profile of the conjugates, but to also allow His227 to remain coordinated during the catalytic cycle and thus to increase the catalytic activity and *ee*.

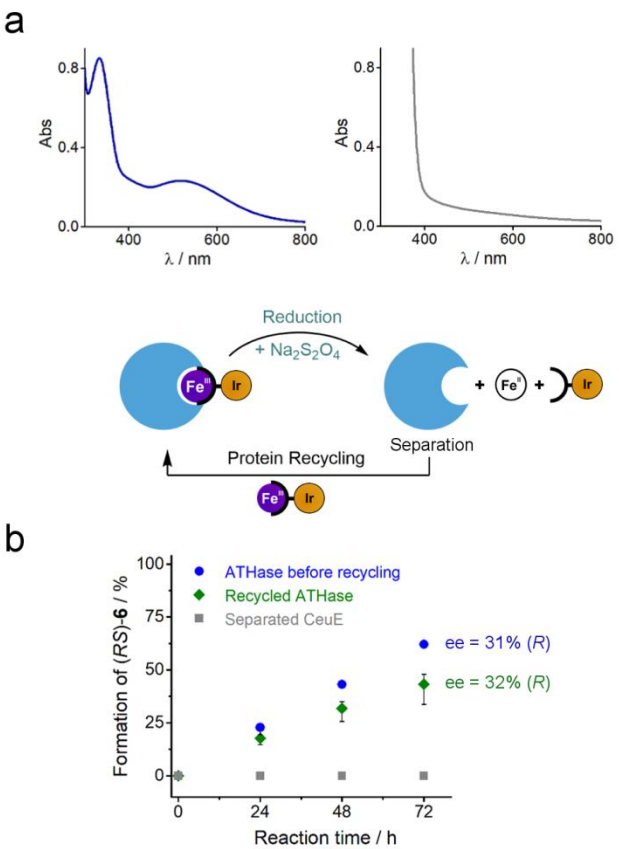

Figure 6. Redox-switchable anchoring enables CeuE recycling. a, Reduction-triggered dissociation of [Fe^{III}(**11**)Cp*Ir^{III}]⊂CeuE followed by CeuE recovery and ATHase re-assembly, as monitored by absorption spectroscopy ([Fe^{III}(**11**)Cp*Ir^{III}]⊂CeuE λ_{max} = 547 nm): CeuE (blue), iron(III) (purple), azotochelin with attached catalyst (black + yellow), iron(II) (white/grey); 0.1 M

MES, pH 6.0, 0.5 M NaCl. **b**, Catalytic assay conditions as in Figure 5, but with reduced catalyst concentration of 0.05 mM (0.1 mol%) ATHase (experiments with recycled CeuE were performed in triplicate, error bars show min. and max. values).

CONCLUSIONS

We have identified azotochelin and CeuE as a siderophore-protein combination that allows an iridium-based transfer hydrogenation catalyst to be anchored both strongly and reversibly, *via* the iron complex of the siderophore. Proof-of-concept was demonstrated by means of a prototype ATHase, [Fe^{III}(**11**)Cp*Ir^{III}]⊂CeuE, which was characterised by mass spectrometry, CD spectroscopy and X-ray crystallography and shown to catalyse the reduction of a prochiral imine with reproducible enantioselectivity. The crystal structure of the ATHase revealed that His227 is located close to the catalytic iridium(III) centre. This observation, together with the fact that its replacement with alanine results in a clear decrease in *ee* strongly suggests that His227 forms a key part of the chiral binding pocket responsible for the enantioselectivity.

Since the product obtained in the absence of the protein scaffold is essentially racemic, the transfer hydrogenation reaction provided a means of differentiating the CeuE-bound state of the siderophore-catalyst conjugate from its unbound state. This demonstrates that the insertion of the conjugate into the protein scaffold can be controlled *via* the oxidation state of the iron. In the presence of iron(III), the azotochelin-based anchor binds strongly to CeuE, but the anchor can be released *via* reduction of iron(III) to iron(II).

In this way, catalytic centres that have lost activity, for example due to poisoning or decomposition, could easily be removed and then replaced by a new active catalyst, thereby allowing the protein scaffold to be reused. In addition, there is scope for the introduction of other catalysts with similar piano-stool structures. Hence, we propose that the redox-switchable nature of ferric-azotochelin anchoring, if combined with a modular approach to enzyme design, could

extend the range of applications in which artificial enzymes can be utilised. If, for example, CeuE was to be immobilised on a surface, controlled redox switching, either electrochemically or chemically, could be used to reversibly bind a chosen catalyst where and when required, allowing biosensor arrays or discovery flow systems to be developed. Catalyst exchange *via* redox switching would thus allow the re-patterning and re-programming of a given platform.

Opportunities to widen the scope of the reversible anchoring approach include the exploration of similar tetradentate siderophores, initially in combination with other catecholate siderophore-binding proteins, in particular those with iron-coordinating Tyr and His residues. [29, 30] Looking forward, it would be of interest to engineer suitable amino acid combinations into the binding pockets of unrelated proteins. Therefore, our feasibility study is expected to open up interesting new prospects in artificial enzyme research.

METHODS

Compound synthesis and characterisation:

General methods. ^{1}H and ^{13}C NMR spectra were recorded on a Jeol ECS 400 (400 MHz for ^{1}H, 100 MHz for ^{13}C) at ambient temperature. Chemical shifts are reported relative to residual solvent peaks and coupling constants (J) are given in Hz. High resolution electrospray ionization (ESI) mass spectra were recorded on a Bruker microTOF electrospray mass spectrometer. Infra-red (IR) spectra were recorded on a PerkinElmer Spectrum Two (ATIR), covering a wavenumber range of 4000-450 cm^{-1}. Elemental analyses were carried out on an Exeter CE-440 elemental analyser. The circular dichroism spectroscopic measurements were performed on a Jasco J810 CD spectropolarimeter at 20 °C under constant nitrogen flush and the specific rotation was recorded on a Jasco DIP-370 digital polarimeter. Fluorescence spectra were recorded on a Hitachi F-4500 fluorescence spectrophotometer. Analytical thin layer chromatography was performed using Merck silica gel 60 F253 aluminium-backed plates using specified

solvent systems and visualised using a Chromato-vue Model CC-10 ultraviolet lamp. Flash column chromatography was carried out using Fluka Silica, pore size 60 Å, 220-440 mesh, 35-75 µm.

Compound 8. 4-Cyanobenzenesulfonyl chloride (**7**, 11 mmol, 2.21 g) suspended in 100 mL of dichloromethane was added dropwise to a stirred solution of 2-(aminomethyl)pyridine (10 mmol, 1 mL) and triethylamine (20 mmol, 2.8 mL) in 250 mL dichloromethane cooled on ice. The solution was allowed to warm to room temperature over 4 hours and stirred overnight. The solution was concentrated to approximately 100 mL and washed with water (3 x 30 mL) followed by brine (1 x 25 mL). The organic layer was dried with $MgSO_4$ and the solvent dried *in vacuo*. The crude product was recrystallised with hot ethyl acetate using hexanes as an anti-solvent to afford **8** as a beige powder (2.13 g, 7.84 mmol, 78%).

TLC ($CHCl_3$:MeOH, 10:1 v/v): R_f = 0.43; ^{1}H NMR (400 MHz, $(CD_3)_2SO$): δ 8.64 (t, J = 6.0 Hz, 1H), 8.38 (d, J = 4.4 Hz, 1H), 8.02 (d, J = 8.0 Hz, 2H), 7.91 (d, J = 8.8 Hz, 2H), 7.70 (td, J = 7.4, 2.0 Hz, 1H), 7.30 (d, J = 8.4 Hz, 1H), 7.22 (dd, J = 7.2, 5.2 Hz, 1H), 4.16 (d, J = 6.4 Hz, 2H); ^{13}C NMR (100 MHz, $(CD_3)_2SO$): δ 156.6, 148.8, 144.9, 136.7, 133.3, 127.3, 122.5, 121,8, 117.8, 114.7, 47.9; IR (ATIR): 2233 cm^{-1} (CN); HRMS (*m/z*): $[M+H]^+$ calcd. for $C_{13}H_{11}N_3O_2S$, 274.0645; found, 274.0643; analysis (calcd., found for $C_{13}H_{11}N_3O_2S$): C(57.13, 56.94), H(4.06, 4.20), N(15.37, 15.15).

Compound 9. A solution of **8** (2.7 mmol, 0.744 g) in 15 mL dry THF was placed under a nitrogen atmosphere. Lithium borohydride (27.2 mmol, 6.8 mL of a 4 M THF solution, Acros Organics) was added to this stirred solution and the resulting solution was heated to reflux. Once at reflux, dry methanol (81 mmol, 3.3 mL) was added over approximately 5 hours (gas evolution upon addition) and the solution was refluxed overnight under a nitrogen atmosphere. This was followed by addition of an extra 5 mL of dry methanol before the solution was slowly cooled to

room temperature. Deionised water (33 mmol, 0.6 mL) was added and the mixture stirred for one hour before the flask was opened to atmosphere. $MgSO_4$ was added, and the suspension filtered. The solvent was removed *in vacuo* to yield a crude white solid, which was suspended in EtOAc:MeOH (2:1, v:v) and applied to a short silica plug, washed with EtOAc (100%), and the product eluted with EtOAc:MeOH (2:1, v:v). The solvent was removed *in vacuo* to yield **9** in form of a white solid (0.531 g, 1.91 mmol, 70%).

TLC (EtOAc 100%): $R_f = 0$; ^{1}H NMR (400 MHz, $(CD_3)_2SO$): δ 8.43 (d, $J = 5.0$ Hz, 1H), 7.75-7.71 (m, 3H), 7.51 (d, $J = 8.0$ Hz, 2H), 7.36 (d, $J = 7.5$ Hz, 1H), 7.24 (dd, $J = 7.0, 5.0$ Hz, 1H), 4.04 (s, 2H), 3.77 (s, 2H); ^{13}C NMR (100 MHz, $(CD_3)_2SO$): δ 157.2, 149.2, 148.8, 138.2, 136.7, 127.5, 126.4, 122.4, 121.6, 47.9, 45.2; HRMS (*m/z*): $[M+H]^+$ calcd. for $C_{13}H_{15}N_3O_2S$, 278.0958; found, 278.0948, analysis (calcd., found for $C_{62}H_{56}N_2O_{11}.0.25H_2O$): C(73.76, 73.46), H(5.64, 5.51), N(2.77, 2.79).

Compound 10. 1-Ethyl-3-(3-dimethylaminopropyl)carbodiimide (0.5 mmol, 90 µL) was added to a stirred solution of Bn_4-azotochelin (0.5 mmol, 0.389 g, prepared in accordance to the literature[46]), triethylamine (1 mmol, 0.139 mL) and hydroxybenzotriazole (0.05 mmol, 6.75 mg) in 5 mL dry DMF. Subsequently **9** (0.5 mmol, 0.138 g) was added and the solution was stirred overnight with a drying tube attached. The DMF was removed *in vacuo* and the crude product was suspended in 75 mL ethyl acetate and washed with 0.1 M HCl (1 x 25 mL), saturated $NaHCO_3$ (1 x 25 mL) and brine (1 x 25 mL). The organic layer was dried over $MgSO_4$ and the solvent dried *in vacuo*. The crude product was purified by column chromatography (silicagel, 100% EtOAc) to afford the pure **10** as an off-white powder (0.244 g, 0.235 mmol, 47%).

TLC (EtOAc 100%): $R_f = 0.17$; ^{1}H NMR (400 MHz, $CDCl_3$): δ 8.43 (d, $J = 7.0$ Hz, 1H), 8.39 (d, $J = 4.5$ Hz, 1H) 7.95 (t, $J = 5.5$ Hz, 1H), 7.70 (d, $J = 8$ Hz, 2H), 7.63 (dt, $J = 7.0, 3.0$ Hz, 2H), 7.54 (td, $J = 8.0, 1.5$ Hz, 1H), 7.49-7.24 (m, 23H), 7.18-7.08 (m, 6H), 6.23 (m, 1H), 5.14 (app s,

4H), 5.10 (s, 2H), 5.04 (s, 2H), 4.46 (q, *J* = 7.0 Hz, 1H), 4.40 (d, *J* = 6.5 Hz, 2H), 4.18 (d, J = 2.5 Hz, 2H), 3.14 (q, J = 6.5 Hz, 2H), 1.70 (app sext., J = 7.5 Hz, 1H), 1.39-1.12 (m, 5H); ^{13}C NMR (100 MHz, $CDCl_3$): δ 171.7, 165.7, 165.0, 154.8, 151.7, 151.6, 148.8, 146.8, 146.6, 143.5, 138.3, 136.7, 136.3, 136.3, 136.1, 136.0, 128.9, 128.7, 128.7, 128.6, 128.6, 128.3, 128.2, 127.8, 127.7, 127.6, 127.3, 127.1, 126.3, 124.4, 124.4, 123.1, 122.9, 122.5, 121.9, 117.3, 116.8, 76.3, 76.1, 71.3, 71.2, 53.6, 47.4, 42.6, 39.0, 30.6, 28.8, 23.1; HRMS (*m/z*): $[M+H]^+$ calcd. for $C_{61}H_{59}N_5O_9S$, 1038.4106; found, 1038.4114; analysis (calcd., found for $C_{61}H_{59}N_5O_9S.0.5H_2O$): C(69.96, 70.02), H(5.77, 5.74), N(6.69, 6.51).

Compound 11. Reaction glassware was prepared by soaking in 6 M HCl for 4 hours, followed by potassium hydroxide in EtOH to remove any residual metal ions. To a solution of **10** (0.09 mmol, 93 mg) dissolved in dry ethanol, palladium hydroxide 20% on carbon (0.1 mmol, 70 mg) was added. The vessel was purged with nitrogen, followed by hydrogen and then filled with hydrogen. The reaction was stirred vigorously overnight. The remaining hydrogen was released and the suspension filtered using a Whatman® Glass Microfiber Filter GF/F. The organic solvent was removed *in vacuo* to yield **11** as a beige solid (57.7 mg, 0.085 mmol, 95%).

TLC (EtOAc, 100%): R_f = 0; ^{1}H NMR (400 MHz, CD_3OD): δ 8.34 (d, *J* = 6.0 Hz, 1H), 7.74 (d, *J* = 8.4 Hz, 2H), 7.68 (td, *J* = 7.8, 2 Hz, 1H), 7.43 (d, *J* = 8.4 Hz, 2H), 7.36-7.32 (m, 2H), 7.22-7.17 (m, 2H), 6.94-6.90 (m, 2H), 6.73-6.66 (m, 2H), 4.60-4.57 (m, 1H), 4.48-4.39 (m, 2H), 4.15 (s, 2H), 3.61 (q, J = 7.0, 1.8H, EtOH), 3.39 (t, *J* = 7.0 Hz, 2H), 1.98-1.85 (m, 2H), 1.72-1.64 (m, 2H), 1.59-1.48 (m, 2H), 1.18 (t, J = 7.0 Hz, 2.8H, EtOH); ^{13}C NMR (100 MHz, CD_3OD): δ 173.4, 170.2, 169.8, 156.9,148.9, 148.4, 148.2, 146.0, 145.9, 143.9, 139.1, 137.5, 127.6, 126.9, 122.7, 122.2, 118.5, 118.3, 118.2, 117.3, 115.7, 115.5, 57.0 (EtOH), 53.9, 47.5, 42.2, 38.8, 31.3, 28.7, 23.1, 17.05 (EtOH); HRMS (*m/z*): $[M-H]^-$ calcd. for $C_{33}H_{34}N_5O_9S$, 676.2083; found, 676.2067; analysis (calcd., found for $C_{33}H_{35}N_5O_9S.0.8EtOH.1.8H_2O.0.2KCl$): C(54.54, 54.89), H(5.74, 5.45), N(9.19, 8.84).

Compound 12. $[Ir(Cp^*)(Cl)_2]_2$ (0.1 mmol, 0.0799 g, prepared in accordance with the literature[47]) was dissolved in 2 mL dichloromethane and added to a stirred solution of **8** (0.2 mmol, 0.0550 g) in 1 mL dichloromethane. Sodium hydroxide (0.1 mL, 2.0 M methanolic) was added to give a pale orange/yellow solution, which was stirred for one hour. The solution was filtered and the solvent removed *in vacuo* to give an orange solid, which was washed with di-ethyl ether (3 x 5 mL) to yield **12** as a pale orange solid (0.0743 g, 0.11 mmol, 55%).

^{1}H NMR (400 MHz, $CDCl_3$): δ 8.54 (d, *J* = 5.5 Hz, 1H), 8.15 (d, *J* = 8.5 Hz, 2H), 7.72 (app. t, *J* = 7.5 Hz, 1H), 7.58 (d, *J* = 8.0 Hz, 2H), 7.29-7.23 (m, 2H), 4. 85 (d, *J* = 17.0 Hz, 1H), 4.54 (d, *J* = 17.0 Hz, 1H), 1.73 (s, 15H). ^{13}C NMR (100 MHz, $CDCl_3$): δ 163.9, 151.5, 148.0, 138.5, 132.4, 129.2, 125.2, 120.7, 118.7, 114.1, 87.1, 57.8, 9.8; IR (ATIR): 2230 cm^{-1} (CN); HRMS (*m/z*): $[M\text{-}Cl]^+$ calcd. for $^{191}IrC_{23}H_{25}N_3O_2S$, 598.1268; found, 598.1268.

The ^{1}H and ^{13}C NMR spectra of compounds **8-12** are shown in Supplementary Fig. 10.

Site-directed mutagenesis and purification of CeuE. The plasmid encoding N-terminal hexahistidine-tagged CeuE used in previous studies[30] was isolated from *E. coli* NovaBlue competent cells (Merck Chemicals Ltd) using a Wizard® Genomic DNA Purification kit (Promega). Site-directed mutagenesis was performed in a 25 µl reaction containing Kod Hot start DNA polymerase (0.5 U), dNTPs (200 µM), $MgSO_4$ (1 mM), plasmid DNA (1 ng), forward primer (5'-CTGTTCCAGGGACCAGCATTGTTGCCTATTAGTA) (400 µM), reverse primer (5'-TACTAATAGGCAACAATGCTGGTCCCTGGAACAG) (400 µM), and 1 x Kod PCR buffer. The PCR cycle was performed at 94°C for 2 minutes, followed by 18 cycles of 94 °C for 30 s, 60 °C for 30 s, and 72°C for 3 minutes, followed by a final extension at 72 °C for 5 minutes. The template DNA was removed by addition of 2 µL of CutSmart® buffer and 1µL DpnI (20 U/µL) to 20 µL of PCR reaction followed by incubation at 37 °C for 2 hours. The final PCR product was transformed into NovaBlue competent cells. Mutagenesis was confirmed by isolation and

sequencing of the plasmid from several bacterial colonies using a T7 promoter primer (Eurofins MWG operon). Protein from mutated plasmids was expressed in *E. coli* BL21 (DE3) cells grown in Luria-Bertani broth with 50 µg/mL kanamycin. Cultures were grown at 37 °C with shaking at 200 rpm. When the OD_{600} reached 0.6, protein expression was induced by addition of 1 mM IPTG to cultures. Cultures were further incubated for 4 hours and cells were harvested by centrifugation. Cell pellets were resuspended 1:10 (w/v) in 50 mM Tris-Cl pH 7.5, 500 mM NaCl, 10 mM imidazole with cOmplete™ EDTA-free Protease Inhibitor Cocktail (Roche Diagnostics) followed by sonication. The lysate was cleared of insoluble material by centrifugation at 38,000 x *g*, 4°C for 40 min followed by filtration of supernatant through a 0.4 µm syringe filter. The filtered sample was loaded onto a 5 mL HisTrap™ FF Ni-chelating column (GE healthcare) and eluted using an imidazole gradient (final concentration of 500 mM) on a Bio-Rad NGC™ chromatography system. The N-terminal histidine tag was removed by addition of 2 mg of 3C protease to 100 mg of eluate, followed by dialysis in 3 L of 40 mM Tris-Cl pH 7.5, 150 mM NaCl at 4°C for 16 h. Residual traces of His-tagged CeuE and 3C protease were removed from the sample by repeating the Ni-affinity purification step. Protein samples were dialysed twice in 2 L of 100 mM MES pH 6, 500 mM NaCl at 4°C for 20 h. Protein was concentrated to 60 mg/mL in an Amicon centrifugation filter unit (Millipore), separated into 50 µL aliquots and stored at -80 °C. Protein purity and integrity was confirmed by SDS-PAGE and UV-CD.

CeuE with a mutation at the histidine at position 227 to alanine was prepared as described in a previous study.[43]

Preparation of the artificial transfer hydrogenase [Fe^{III}(11)Cp*Ir^{III}]⊂CeuE. First, [$Fe^{III}(solv)_2$(**11**)Cp*$Ir^{III}Cl$]$^-$ was formed by adding 60 µL of a 10 mM Fe(III)-NTA solution (prepared as previously described[29]) to 18 µL of 200 mM MOPS pH 7.5, 150 mM NaCl and

incubation in a sonication bath for 10 minutes. Following this, **11** (12 µL, 50 mM in DMF) was added and the mixture was sonicated for 10 minutes. Then, $[Cp^*Ir^{III}Cl_2]_2$ (30 µL, 10 mM in DMF) was added and the mixture was sonicated for 10 minutes. $[Fe^{III}(\mathbf{11})Cp^*Ir^{III}]\subset$CeuE was subsequently formed by addition of 250 µL of 60 mg/ml CeuE to 15 mL of 100 mM MES pH 6, 500 mM NaCl, followed by addition of 96.5 µL of the $[Fe^{III}(solv)_2(\mathbf{11})Cp^*Ir^{III}Cl]^-$ solution. The resulting solution was concentrated in a Vivaspin 20 centrifugation filter unit (3 kDa MWCO) and the protein concentration was determined using a Pierce™ Coomassie Plus (Bradford) Assay kit (Thermofisher) using BSA as a standard.

Catalytic activity testing:

General. 6,7-dimethoxy-1-methyl-3,4-dihydroisoquinoline was purchased from Acros. Analytical HPLC measurements were performed on a Shimadzu HPLC system (Prominence) equipped with a LC-20AD pump, SIL-20A autosampler, DGU-20AS degasser, CTO-20AC column oven, CBM-20A communication bus module and SPD-M20A diode array detector using a Lux Cellulose-4 column (Phenomenex, 250 mm x 4.6 mm, 5 µm) with the specified eluent gradient.

Stock solutions. MES/formate buffer: 6.40 g of 2-morpholin-4-ylethanesulfonic acid monohydrate (MES monohydrate) and 10.20 g of sodium formate were dissolved in 40 mL water and the pH adjusted by addition of NaOH, before the solution volume was finalised at 50 mL (final concentration 0.6 M MES, 3 M formate). Substrate: 0.2053 g of 6, 7-dimethoxy-1-methyl-3,4-dihydroisoquinoline was dissolved in 2 mL of MES/formate buffer (final concentration 0.5 M). Compound **11**: 3.39 mg of **11** was dissolved in 500 µL DMF (final concentration 10 mM). Glutathione: 76.8 mg of glutathione was dissolved in 1 mL of water (final concentration 250 mM).

Catalyst. 10 mM stock solutions of the required catalysts were prepared *in situ* by mixing $[IrCp^*Cl_2]_2$ with the appropriate ligand in DMF.

General procedure. 6,7-dimethoxy-1-methyl-3,4-dihydroisoquinoline (50 mM) and 0.125 mM catalyst in 0.6 M MES pH 6, 3 M sodium formate incubated at 40°C with a magnetic stirrer set to 400 rpm. Reactions were initiated by addition of the substrate and 25 µL samples were taken at selected time points and quenched by adding to 975 µL of L-glutathione (50 µL of 250 mM L-glutathione stock diluted in 300 µL water and 625 µL MeOH). Samples were left to stand for 1 hour at 4 °C before being filtered through 0.22 µm nylon membranes. Reaction progression was monitored *via* HPLC (see HPLC method below for further details). Peaks that represented substrate and product with an absorbance at 285 nm were integrated and used to calculate normalised product percentages.

HPLC method. Solvent A: H_2O + 0.1% DEA, solvent B : MeCN + 0.1% DEA. The starting ratio was 75:25 (A:B) and was maintained for 12 minutes. Ramp to 35:65 (A:B) at 12 minutes over 0.5 minutes and held for 2.5 minutes. At 15 minutes the solvent was ramped back to 75:25 (A:B) over 0.5 minutes amd held until 35 minutes. 1 mL/min, 35 °C; T_R (*S*)-(-)-Salsolidine 11.5 min, (*R*)-(+)-Salsolidine 12.5 min, 6,7-dimethoxy-1-methyl-3,4-dihydroisoquinoline 15.5 min.

Data availability. Experimental details of circular dichroism spectroscopic measurements (Fig. 4b), intrinsic fluorescence quenching titrations (Fig. 4a), mass spectrometry measurements, crystal structure determinations (Fig. 4c-e) and reversibility studies (Figs. 2, 6) are described in the Supplementary Methods. X-ray crystallographic data are available in the EMBL-EBI PDB under the accession numbers 5OAH ($[Fe^{III}(AZOTO)]^{2-}$⊂CeuE) and 5OD5 $[Fe^{III}(\mathbf{11})Cp^*Ir^{III}]$⊂CeuE and the Cambridge Crystallographic Data Centre deposition number

CCDC 1551724 (**12**). Other supporting data were deposited with the University of York library (www.york.ac.uk/library/info-for/researchers/datasets/) under DOI: 10.15124/233cf8cc-d25a-4793-b667-7557836774c1 or are available from the authors upon reasonable request.

Acknowledgements

We thank the Engineering and Physical Sciences Research Council (EPSRC, grant EP/L024829/1) and Biotechnology and Biological Sciences Research Council (BBSRC) for financial support, the Diamond Light Source for access to beamlines I03 and I04 (proposal; mx-13587) and J. Turkenburg and S. Hart for assistance with data collection. In addition, experimental support by K. Heaton (mass spectrometry), A. Leech (CD spectroscopy and mass spectrometry), A. Dixon (HPLC), J. H. Peng (catalyst preparation) and A. C. Whitwood (small-molecule crystallography) is gratefully acknowledged.

Author contributions

The experiments were performed by D.J.R. (chemical synthesis, development of catalysts and screening protocols, binding constant determination, redox reversibility tests), J.E.C. (artificial enzyme production and characterization, catalytic screening, redox reversibility tests), A.-K. D.-K. (redox reversibility tests), E.V.B. (protein production and protein crystal growth), E.J.D (protein crystal structure refinement) and K.S.W. (protein crystal structure refinement). K.S.W. (structural biology) and A.-K.D.-K. (chemistry) supervised and directed the project. The manuscript was produced by D.J.R and A.-K.D.-K. based on contributions by all authors. All authors have given approval to the final version of the manuscript.

Competing interests

The authors declare no competing interests.

REFERENCES

(1) Hoarau, M., Hureau, C., Gras, E. & Faller, P. Coordination complexes and biomolecules: a wise wedding for catalysis upgrade. *Coord. Chem. Rev.* **308**, 445-459 (2016).

(2) Yu, F. *et al.* Protein design: toward functional metalloenzymes. *Chem. Rev.* **114**, 3495-3578 (2014).

(3) Lu, Y., Yeung, N., Sieracki, N. & Marshall, N.M. Design of functional metalloproteins. *Nature* **460**, 855-862 (2009).

(4) Lewis, J.C. Artificial metalloenzymes and metallopeptide catalysts for organic synthesis. *ACS Catal.* **3**, 2954-2975 (2013).

(5) Bos, J. & Roelfes, G. Artificial metalloenzymes for enantioselective catalysis. *Curr. Opin. Chem. Biol.* **19**, 135-143 (2014).

(6) Matsuo, T. & Hirota, S. Artificial enzymes with protein scaffolds: structural design and modification. *Biorg. Med. Chem.* **22**, 5638-5656 (2014).

(7) Pàmies, O., Diéguez, M. & Bäckvall, J.-E. Artificial metalloenzymes in asymmetric catalysis: key developments and future directions. *Adv. Synth. Catal.* **357**, 1567-1586 (2015).

(8) Heinisch, T. & Ward, T.R. Artificial metalloenzymes based on the biotin–streptavidin technology: challenges and opportunities. *Acc. Chem. Res.* **49**, 1711-1721 (2016).

(9) Sauer, D.F. *et al.* A highly active biohybrid catalyst for olefin metathesis in water: Impact of a hydrophobic cavity in a β-barrel protein. *ACS Catal.* **5**, 7519-7522 (2015).

(10) Cotelle, Y., Lebrun, V., Sakai, N., Ward, T.R. & Matile, S. Anion-π enzymes. *ACS Cent. Sci.* **2**, 388-393 (2016).

(11) Schwizer, F. *et al.*T. R. Artificial metalloenzymes: Reaction scope and optimization strategies. *Chem. Rev.* **118**, 142-231 (2018).

(12) Jeschek, M., Panke, S., Ward, T. R. Artificial metalloenzymes on the verge of new-to-nature metabolism. *Trends Biotechnol.* **36**, 60-72 (2018).

(13) Wilson, M.E. & Whitesides, G.M. Conversion of a protein to a homogeneous asymmetric hydrogenation catalyst by site-specific modification with a diphosphinerhodium(I) moiety. *J. Am. Chem. Soc.* **100**, 306-307 (1978).

(14) Jeschek, M. *et al.* Directed evolution of artificial metalloenzymes for in vivo metathesis. *Nature* **537**, 661-665 (2016).

(15) Hyster, T.K., Knörr, L., Ward, T.R. & Rovis, T. Biotinylated Rh(III) complexes in engineered streptavidin for accelerated asymmetric C–H activation. *Science* **338**, 500-503 (2012).

(16) Liu, Z. et al. Upregulation of an artificial zymogen by proteolysis. *Angew. Chem. Int. Ed*. **55**, 11587-11590 (2016).

(17) Monnard, F.W., Nogueira, E.S., Heinisch, T., Schirmer, T. & Ward, T.R. Human carbonic anhydrase II as host protein for the creation of artificial metalloenzymes: the asymmetric transfer hydrogenation of imines. *Chem. Sci.* **4**, 3269-3274 (2013).

(18) Matsuo, T. *et al.* Creation of an artificial metalloprotein with a Hoveyda-Grubbs catalyst moiety through the intrinsic inhibition mechanism of a-chymotrypsin. *Chem. Commun.* **48**, 1662-1664 (2012).

(19) Key, H.M., Dydio, P., Clark, D.S. & Hartwig, J.F. Abiological catalysis by artificial haem proteins containing noble metals in place of iron. *Nature* **534**, 534-537 (2016).

(20) Ying, L.-Q. Branchaud, B.P. Design of a reversible biotin analog and applications in protein labeling, detection, and isolation. *Chem. Commun*. **47**, 8593-8595 (2011).

(21) Terai, T. *et al.* Artificial ligands of streptavidin (ALiS): Discovery, characterization, and application for reversible control of intracellular protein transport. *J. Am. Chem. Soc.* **137**, 10464-10467 (2015).

(22) Pollheimer, P. *et al.* Reversible biofunctionalization of surfaces with a switchable mutant of avidin. *Bioconjugate Chem.* **24**, 1656-1668 (2013).

(23) Dwyer, M. A., Hellinga, H. W. Periplasmic binding proteins: a versatile superfamily for protein engineering. *Curr. Opin. Struct. Biol.* **14**, 495-504 (2004).

(24) Miethke, M. & Marahiel, M.A. Siderophore-based iron acquisition and pathogen control. *Microbiol. Mol. Biol. Rev.* **71**, 413-451 (2007).

(25) Hider, R.C. & Kong, X. Chemistry and biology of siderophores. *Nat. Prod. Rep.* **27**, 637-657 (2010).

(26) Schalk, I.J. & Guillon, L. Fate of ferrisiderophores after import across bacterial outer membranes: different iron release strategies are observed in the cytoplasm or periplasm depending on the siderophore pathways. *Amino Acids* **44**, 1267-1277 (2013).

(27) Wilson, B.R., Bogdan, A.R., Miyazawa, M., Hashimoto, K. & Tsuji, Y. Siderophores in iron metabolism: from mechanism to therapy potential. *Trends Mol. Med.* **22**, 1077-1090 (2016).

(28) Ganne, G. *et al.* Iron release from the siderophore pyoverdine in *Pseudomonas aeruginosa* involves three new actors: FpvC, FpvG, and FpvH. *ACS Chem. Biol.* **12**, 1056-1065 (2017).

(29) Raines, D.J. *et al.* Bacteria in an intense competition for iron: key component of the *Campylobacter jejuni* iron uptake system scavenges enterobactin hydrolysis product. *Proc. Natl. Acad. Sci. U.S.A.* **113**, 5850-5855 (2016).

(30) Raines, D.J., Moroz, O.V., Wilson, K.S. & Duhme-Klair, A.-K. Interactions of a periplasmic binding protein with a tetradentate siderophore mimic. *Angew. Chem. Int. Ed.* **52**, 4595-4598 (2013).

(31) Zimbron, J.M. *et al.* A dual anchoring strategy for the localization and activation of artificial metalloenzymes based on the biotin–streptavidin technology. *J. Am. Chem. Soc.* **135**, 5384-5388 (2013).

(32) Dürrenberger, M. *et al.* Artificial transfer hydrogenases for the enantioselective reduction of cyclic imines. *Angew. Chem. Int. Ed.* **50**, 3026-3029 (2011).

(33) Madern, N., Talbi, B. & Salmain, M. Aqueous phase transfer hydrogenation of aryl ketones catalysed by achiral ruthenium(II) and rhodium(III) complexes and their papain conjugates. *Appl. Organomet. Chem.* **27**, 6-12 (2013).

(34) Chimiak, A. & Neilands, J.B. Lysine analogues of siderophores. *Struct. Bond.* **58**, 89-96 (1984).

(35) Lo, C., Ringenberg, M.R., Gnandt, D., Wilson, Y. & Ward, T.R. Artificial metalloenzymes for olefin metathesis based on the biotin-(strept)avidin technology. *Chem. Commun.* **47**, 12065-12067 (2011).

(36) Stookey, L. L., Ferrozine - A new spectrophotometric reagent for iron. *Anal. Chem.* **42**, 779-781 (1970).

(37) Ruff, A., Kirby, C., Chan, B. C., O'Connor, A. R. Base-free transfer hydrogenation of ketones using Cp*Ir(pyridinesulfonamide)Cl precatalysts. *Organometallics* **35**, 327-335 (2016).

(38) Townsend, T. M., Kirby, C., Ruff, A., O'Connor, A. R., Transfer hydrogenation of aromatic and linear aldehydes catalyzed using Cp*Ir(pyridinesulfonamide)Cl complexes under base-free conditions. *J. Organomet. Chem.* **843**, 7-13 (2017).

(39) Fu, Y. *et al.*The contrasting catalytic efficiency and cancer cell antiproliferative activity of stereoselective organoruthenium transfer hydrogenation catalysts. *Dalton Trans.* **45**, 8367-8378 (2016).

(40) Soni, R. *et al.* The importance of the N-H bond in Ru/TsDPEN complexes for asymmetric transfer hydrogenation of ketones and imines. *Org. Biomol. Chem.* **9**, 3290-3294 (2011).

(41) Václavík, J. *et al.* Experimental and theoretical perspectives of the Noyori-Ikariya asymmetric transfer hydrogenation of imines. *Molecules* **19**, 6987-7007 (2014).

(42) Müller, A., Wilkinson, A.J., Wilson, K.S. & Duhme-Klair, A.-K. An $[\{Fe(mecam)\}_2]^{6-}$ bridge in the crystal structure of a ferric enterobactin binding protein. *Angew. Chem. Int. Ed.* **45**, 5132-5136 (2006).

(43) Wilde, E.J. *et al.* Interactions of the periplasmic binding protein CeuE with Fe(III) n-LICAM^{4-} siderophore analogues of varied linker length. *Sci. Rep.* **7**, 45941 (2017).

(44) Scarrow, R.C., Ecker, D.J., Ng, C., Liu, S. & Raymond, K.N. Iron(III) coordination chemistry of linear dihydroxyserine compounds derived from enterobactin. *Inorg. Chem.* **30**, 900-906 (1991).

(45) Okamoto, Y., Köhler, V. & Ward, T.R. An NAD(P)H-dependent artificial transfer hydrogenase for multienzymatic cascades. *J. Am. Chem. Soc.* **138**, 5781-5784 (2016).(46) Chimiak, A. & Neilands, J.B. Lysine analogues of siderophores. *Struct. Bond.* **58**, 89-96 (1984).

(47) White, C., Yates, A., Maitlis, P. M., & Heinekey, D. M. (η^5-Pentamethylcyclopentadienyl) rhodium and-iridium compounds. *Inorg. Synth.* **29**, 228-234 (2007).